MASARYKOVA UNIVERZITA
Přírodovědecká fakulta
Ústav teoretické fyziky a astrofyziky

Bakalářská práce

Brno 2025 Barbora Hudačková

MASARYKOVA
UNIVERZITA
PŘÍRODOVĚDECKÁ FAKULTA
ÚSTAV TEORETICKÉ FYZIKY A ASTROFYZIKY

Analysis of time delay of gamma-ray bursts

Bakalářská práce

Barbora Hudačková

Vedoucí práce: Mgr. Samuel Kováčik, Ph.D. **Brno 2025**

Bibliografický záznam

Autor:	Barbora Hudačková Přírodovědecká fakulta, Masarykova univerzita Ústav teoretické fyziky a astrofyziky

Název práce:	Analýza časového spoždení gamma zábleku
Studijní program:	Fyzika
Studijní obor:	Astrofyzika
Vedoucí práce:	Mgr. Samuel Kováčik, Ph.D.
Akademický rok:	2024/2025
Počet stran:	xiv + 34
Klíčová slova:	kvantová gravitace; vakuová disperze; gamma záblezky; vzájemná korelácia; chybová korelace; Planckova škála

Bibliographic Entry

Author:	Barbora Hudačková Faculty of Science, Masaryk University Department of Theorethical Physics and Astrophysics

Title of Thesis:	Analysis of time delay of gamma-ray bursts
Degree Programme:	Physics
Field of Study:	Astrophysics
Supervisor:	Mgr. Samuel Kováčik, Ph.D.
Academic Year:	2024/2025
Number of Pages:	xiv + 34
Keywords:	In-vacuo dispersion; Quantum gravity; Gamma-ray bursts; Cross-correlation; Error-correlation; Planck scale

Abstrakt

V této práci představujeme potenciálně pozorovatelný efekt kvantové teorie gravitace, předpověď porušení Lorentzovy invariance při dosažení Planckovy škály. Zaměřujeme se na vákuovú disperzi a provádíme fenomenologickou analýzu rychlosti fotonů v záblescích gama v závislosti na energii jako potenciální signatury disperze v Planckově škále. Vyvíjíme simulační rámec, který generuje syntetické světelné křivky GRB a zavádí lineární časový posun v závislosti na energii. Poté jsme vyhodnotili dvě metody detekce zpoždění: klasickou vzájemnou korelaci, oblíbenou metodu detekce zpoždění v signálech, a novou metodu chybové korelace, která slibuje detekci subbinových zpoždění. Systematicky měníme úroveň šumu, časové rozlišení a vložené zpoždění a mapujeme limity citlivosti každé metody. Uvádíme některé pozorovací požadavky nezbytné k testování rozptylu ve vákuu pomocí současných a připravovaných přístrojů a diskutujeme o budoucnosti fenomenologické kvantové gravitace.

Abstract

In this thesis, we present a potentially observable effect of quantum gravity theory, the prediction of Lorentz invariance violation when reaching the Planck scale. Focusing on an in-vacuo dispersion, we conduct a phenomenological analysis of energy-dependent photon speed in gamma-ray bursts as a potential signature of Planck-scale dispersion. We develop a simulation framework that generates synthetic GRB light curves and imposes a linear energy-dependent time shift. We then evaluated two delay detection methods: classical cross-correlation, a popular method for delay detection in signals, and a novel error-correlation method with a promise of detecting sub-bin delays. By systematically varying noise levels, temporal resolution, and injected delay, we map each method's sensitivity limits. We present some observational requirements necessary to test in-vacuo dispersion with current and upcoming instruments and discuss the future of phenomenological quantum gravity.

MUNI
SCI

MASARYKOVA UNIVERZITA
PŘÍRODOVĚDECKÁ FAKULTA
KOTLÁŘSKÁ 2, 611 37 BRNO
IČ: 00216224
DIČ: CZ00216224

ZADÁNÍ BAKALÁŘSKÉ PRÁCE

Akademický rok: 2024/2025

Ústav:	Ústav teoretické fyziky a astrofyziky
Studentka:	Barbora Hudačková
Program:	Fyzika
Specializace:	Astrofyzika

Ředitel *ústavu* PřF MU Vám ve smyslu Studijního a zkušebního řádu MU určuje bakalářskou práci s názvem:

Název práce:	Analýza časového zpoždění gama záblesků
Název práce anglicky:	Analysis of time delay of gamma-ray bursts
Jazyk práce:	angličtina

Oficiální zadání:
Gama záblesky mají dvě významné vlastnosti. Za prvé, díky intenzitě jejich zdrojů je lze vidět i na gigaparsekové vzdálenosti. Za druhé, díky jejich energii jsou – alespoň mírně – citlivé na efekty Planckovy škály. Efekt kvantové struktury prostoru, narušené Lorentzovské invariance či jiných modifikací Einsteinovy gravitace vede k předpovědi časového zpoždění. Cílem práce je otestovat některé algoritmy na analýzu časového průběhu a zpoždění gama signálů a jejich porovnání v kontextu testování fyziky na Planckově škále.
Gamma-ray bursts have two significant properties. Firstly, due to the intensity of their sources, they can be observed even at gigaparsec distances. Secondly, due to their energy, they are – at least slightly – sensitive to Planck scale effects. The effect of the quantum structure of space, broken Lorentz invariance, or other modifications of Einstein's gravity leads to the prediction of time delay. The aim of the work is to test some algorithms for analysing the time course and delay of gamma signals and to compare them in the context of testing physics at the Planck scale.

Amelino-Camelia, G., Ellis, J., Mavromatos, N. E., Nanopoulos, D. V., & Sarkar, S. (1998). Tests of quantum gravity from observations of gamma-ray bursts. Nature, 393(6687), 763-765. DOI: 10.1038/31647

Vedoucí práce:	Mgr. Samuel Kováčik, Ph.D.
Konzultant:	Bc. Michaela Ďuríšková
Datum zadání práce:	8. 10. 2024
V Brně dne:	10. 5. 2025

Zadání bylo schváleno prostřednictvím IS MU.

Barbora Hudačková, 13. 11. 2024
Mgr. Samuel Kováčik, Ph.D., 18. 11. 2024
RNDr. Luboš Poláček, 4. 12. 2024

Poděkování

V prvom rade by som sa chcela poďakovať môjmu vedúcemu práce Mgr. Samuelovi Kováčikovi, Ph.D. za jeho ochotu, čas a rady pri vypracovávaní tejto práce. Tiež by som sa rada poďakovala aj mojej rodine, kamarátom a priateľovi za podporu a pomoc počas celého štúdia.

Prohlášení

Prohlašuji, že jsem svoji bakalářskou práci vypracoval(-a) samostatně pod vedením vedoucího práce s využitím informačních zdrojů, které jsou v práci citovány.

Brno 13. května 2025 .....

Barbora Hudačková

Contents

Introduction

Modern theoretical physics confronts a profound challenge in unifying the principles of quantum mechanics, which govern the behavior of particles at the smallest scales, with the geometric description of gravity provided by general relativity. A wide class of quantum-gravity theories suggests that, at energies approaching the Planck scale, spacetime itself may exhibit a granular structure, leading to minute deviations in the speed of photon propagation that are too small to detect in terrestrial experiments but could accumulate to observable levels over cosmological distances.

Gamma-ray bursts (GRBs), the most luminous explosions known in the universe, emit brief flashes of photons spanning several orders of magnitude in energy and travel billions of light-years before reaching our detectors, making them ideal cosmic laboratories for testing these tiny dispersion effects.

In this thesis, we address this question by first constructing a flexible, modular simulation of GRB light curves across multiple energy channels: we generate a light curve common to all energies, then impose a controlled, energy-dependent shift in peak arrival times to mimic the effect of in vacuo dispersion, and finally apply Poisson statistics to introduce realistic photon-count fluctuations. We produce a comprehensive synthetic burst dataset varying key observational parameters: signal-to-noise ratio, energy separation between channels, and temporal resolution. We then systematically evaluate two complementary analysis methods on these simulated data. The first is a classical cross-correlation analysis, in which we compute the normalized correlation function between low- and high-energy light curves and identify its maximum as the estimated lag. The second is a novel error-correlation approach: we use the low-energy counts to predict the high-energy counts based on their mean rate ratios, calculate the residuals between predicted and observed high-energy counts, and then examine the lagged autocorrelation of those residuals to reveal delays smaller than a single time bin.

Scanning injected delays from multiple time bins down to fractions of a bin while adjusting noise levels and bin widths, we map the detection limits of each method and quantify how energy bandwidth and timing precision influence sensitivity to Planck-scale dispersion results that clarify the observational requirements for studying these effects and form a basis for applying the pipeline to real GRB data.

Chapter 1

Quantum theory of gravity

The search for a consistent and testable theory of quantum gravity is one of the most important unsolved challenges in fundamental physics. At its core, Quantum gravity aims to combine well-established principles of quantum mechanics, which govern the behavior of particles on the smallest scale, with those of general relativity, which describes the curvature of spacetime and the gravitational interaction on the cosmic scale. Gravity is of a universal nature. Everything is in spacetime, subjected to its geometry, therefore gravity. [1] Einstein's theory so far explains everything from everyday life to the Universe as a whole. The cosmic scales are measured in megaparsecs Mpc or gigaparsecs Gpc. 1Mpc = $3.09 \cdot 10^{22}$m. And the observable universe is estimated to be around 14 Gpc.[2] General relativity is a classical, non-quantum theory. Our current theories for all other interactions are quantum and are described using the quantum framework, which is drastically different from classical physics. Classical mechanics uses trajectories for bodies, and the equations are determined by their initial positions and momentum. Quantum mechanics instead features the wave function, and the relation to position, momentum, or other classical concepts appears via the probability interpretation. Quantum mechanics describes the realm of microphysics, the world of atoms, nuclei, and elementary particles. The smallest scales observed by the Large Hadron Collider are of order 10^{-18}m. Comparing that to the cosmic scale mentioned above, we see that the difference of about 44 orders of magnitude.

1.1 Candidates for Quantum Gravity

Einstein's theory, by itself, is incomplete. General relativity predicts the existence of singularities, such as the centres of black holes or the Big Bang. At these singularities, the predictive power of the theory fails. A quantum theory of gravity is expected to provide a framework in which such singularities are resolved or avoided altogether, offering a more complete description of nature.

A variety of approaches have been proposed to reconcile gravity with quantum mechanics. One of them is a well-known string theory that proposes that the fundamental particles are not point-like but rather one dimensional 'strings' whose vibrational modes give rise to particles and forces. [3] Another candidate is Loop Quantum Gravity (LOQ), which presents a canonical quantisation of general relativity. All of the potential candidates have one thing in common, and that is, they all propose that the space-time itself may have

a structure on a microscopic scale. Scales where we expect quantum effects of gravity to become relevant is the Planck scale derived by Max Planck.

1.1.1 Planck scale

The Planck scale at which the quantum effects and gravitational interactions become intertwined. It is derived from three fundamental constants:

- The speed of light c. The upper limit at which matter or energy can travel through space.
- The Gravitational constant G, presenting a value that fixes the absolute value of interaction strength.
- The reduced Planck constant $\hbar$, is the Planck constant divided by 2π and serves as the fundamental quantum of action in quantum mechanics.

Combining these four constants, we get Planck units like Planck length, time, and mass.

$$l_P = \sqrt{\frac{\hbar G}{c^5}} \approx 1.616 \cdot 10^{-35} m, \tag{1.1}$$

$$t_P = \sqrt{\frac{\hbar G}{c^3}} \approx 5.39 \cdot 10^{-44} s, \tag{1.2}$$

$$m_P = \sqrt{\frac{\hbar c}{G}} \approx 2.18 \cdot 10^{-8} kg. \tag{1.3}$$

For our work, the most important is the derived relation, the Planck energy :

$$E_P = \sqrt{\frac{\hbar c^5}{G}} \approx 1.22 \cdot 10^{28} \text{eV} \tag{1.4}$$

Although this scale is beyond the reach of our current particle accelerators, it serves as a benchmark for the theoretical framework in quantum gravity research. The only apparatus close enough to the Planck energy are Gamma-ray bursts (GRBs).

1.2 Mathematical framework of Quantum Gravity and Noncommutative spacetime

General relativity describes gravity as the curvature of the smooth spacetime, while quantum mechanics governs the behaviour of energy and matter at an extremely small scale. It is expected that at distances approaching the Planck length ($\approx 10^{-35}$m), the concept of continuous spacetime breaks down. Instead, many theories suggest that the space becomes discrete and can be modeled using noncommutative geometry.

In noncommutative spacetime models, introduce a fundamental length scale and alter familiar relationships like the dispersion relation. These modifications are not only of theoretical interest but may also lead to observable effects in astrophysical phenomena.

1.2.1 Noncommutative geomtry

In ordinary quantum mechanics, the commutation between position and momentum:

$$[x, p] = i\hbar \tag{1.5}$$

leads to the Heisenberg uncertainty principle. Similarly, it can be argued, see [4], that at these scales (Planck scale), one can't measure the position of a particle to arbitrary precision. This means that we have two position operators that do not commute.

$$[\hat{x}_i, \hat{x}_j] = i\hat{\Theta}_{ij} \tag{1.6}$$

Natural right-hand side of the equation that is rotationally invariant given by [5] [6] is

$$\hat{\Theta}_{ij} = 2\lambda\,\varepsilon_{ijk}\hat{x}_k, \tag{1.7}$$

where ε is the Levi-cita tensor and λ is a constant with a dimension of length that dictates the scale of space quantumness. In the limit where $\lambda \to 0$, the commutator vanishes and one recovers the original quantum mechanics relation that describes ordinary three-dimensional space.

1.2.2 Modified dispersion relation

In classical relativistic physics, the dispersion relation for massless particles (photons) is given by the well-known equation

$$E^2 = p^2c^2, \tag{1.8}$$

this equation is derived under the assumption that spacetime is continuous, where the coordinates commute and can be precisely measured.

However, assuming the noncommutativity, the concept of an exact position is replaced by uncertainty. Constructing such space, see [5], provides a starting kit for quantum mechanics: the Hilbert space of states Ψ, the position operator $\hat{x}_i$, and the Hamiltonian $\hat{H}$. The velocity was defined in [**?**] and the relation between the velocity operator and the free Hamiltonian has been found,

$$\hat{H}_0 = \frac{1-\sqrt{1-m^2\lambda^2\hat{v}^2}}{m\lambda^2} = \frac{m\hat{v}^2}{2} + \frac{m^3\hat{v}^4}{8}\lambda^2 + \mathcal{O}(\lambda^4). \tag{1.9}$$

The usual relationship is recovered in the limit $\lambda \to 0$. It is plausible that the dispersion law sensitive to the scale of E_f (fundamental energy scale that might be the Planck scale but can be of a different order) will have a similar form, one can replace $\frac{p^2}{2m} \to pc$. Using the Legendre transformation $\hat{p} = \frac{\partial \hat{H}_0}{\partial \hat{v}} = \frac{m\hat{v}}{\sqrt{1-m^2\hat{v}^2\lambda^2}}$, setting the maximal achievable energy to $E_f = 1/m\lambda^2$, therefore $\lambda \to 1/\sqrt{mE_F}$ and considering only energy eigenstates that satisfy $\hat{H}_0\Psi = E\psi$, see [**?**], we obtain the square of energy

$$E^2(p) = E_F^2\left(1-\sqrt{1-\frac{2pc}{E_F+2pc}}\right)^2 = p^2c^2\left(1-\frac{3pc}{E_F}+\mathcal{O}(E_F^{-2})\right). \tag{1.10}$$

This agrees with laws commonly used in other works [7] [8]. The correction term, though small at low energies, may lead to significant observable effects over astronomical distances, as discussed later in 2.1.

Chapter 2

Phenomenology

The quantum gravity problem has been studied for over 90 years [9], assuming that no guidance could be provided from experiment. The Quantum gravity phenomenology focuses on closing the gap between General relativity and quantum mechanics by looking for experimental signatures of a fundamentally quantum space. Instead of waiting for a complete theory of everything to emerge from top-to-bottom theories like string theory or Loop Quantum gravity, we adopt a new bottom-up approach. We develop models that introduce small, often Planck scale suppressed deviations from classical physics and then identify experiments that may amplify these tiny effects into measurable signals.

Quantum gravity phenomology is motivated by the idea that while the Plank scale is extremely small ($\approx 10^{-35}$m), certain experimental context such as the long travel distances or extreme energies of cosmic events can act as natural amplifiers where even the miniscule modification in energy dispersion relation can become detectable. In this thesis, we will mostly focus on the time flight delay, but we will also mention the threshold anomaly.

2.1 Time flight delay

A clear implication of the modified dispersion relation, such as in 1.10, is that the speed at which the waves propagate depends on their wavenumber. The space, due to its granular structure, acts as a dispersive medium for particle propagation. One can imagine such a situation as two photons of two different energies being emitted from the same source simultaneously, but being detected at different times. At first glance, the correlation to the speed of light due to quantum gravity might seem minuscule. For a typical photon with energy $E << E_F$, the correlation is of order E/E_F [9]. In terrestrial experiments, where the E might be in the range MeV-GeV compared to the Planck energy ($\approx 10^{19} GeV$), such effects would be utterly negligible. However, even such a small effect can lead to an observable delay when the photons travel cosmological distances. It is not uncommon for GRB that time-traveled before reaching Earth detectors to be of order $T \sim 10^{17}$s.

2.1.1 Derivation from exact space models

To calculate the flight-time delay from the modified dispersion relation 1.10 according to [5] we first need to replace momentum by the comoving momentum p/a and transform the

velocities using $v = \frac{\partial H}{\partial p}$ and we get

$$v(E) = ca^{-1}\left(\frac{aE_F}{aE_F + 2pc}\right)^{3/2}. \tag{2.1}$$

Next we replace $a = \frac{1}{1+z}$ and integrate to find distance traveled by the received signal

$$x(z,E) = \frac{c}{H_0}\int_0^z \left(\frac{E_F/(1+z')}{E_F/(1+z')+2pc}\right)^{3/2} \frac{dz'}{\sqrt{\Omega_m(1+z')^3+\Omega_\Lambda}}. \tag{2.2}$$

More importantly, we can now calculate the time difference of photons with different energies. So now if $E = pc$

$$\begin{aligned}\Delta t(E_1,E_2,z) = \frac{c}{H_0}\int_0^z &\left(\left(\frac{E_F/(1+z')}{E_F/(1+z')+2p_1c}\right)^{3/2} - \left(\frac{E_F/(1+z')}{E_F/(1+z')+2p_2c}\right)^{3/2}\right) \\ &\cdot \frac{dz'}{\sqrt{\Omega_m(1+z')^3+\Omega_\Lambda}} \\ = -\frac{3c}{H_0}\frac{\Delta E}{E_F}&\int_0^z \frac{(1+z')dz'}{\sqrt{\Omega(1+z'^3)+\Omega}} + \mathcal{O}((E/E_F)^2).\end{aligned} \tag{2.3}$$

2.1.2 Observational considerations

Using the relation 2.3, [5] calculated Δt for the GRB 221109A. This extraordinarily bright GRB was detected in 2022 and its peak luminosity as measured by Fermi Gamma-ray Burst Monitor 10^{47}W over its 1.024s interval [11]. The source of this signal was close with $z = 0.1505$ and the used value for the energy difference was $\Delta E = 99.3$GeV. The cosmological parameters used for the calculation were $H_0 = 67.3\text{km}\cdot\text{s}^{-1}\text{Mps}^{-1}$, $\Omega_m = 0.315$, $\Omega_\Lambda = 0.685$, and for the cut-off energy $E_F \approx E_p$. With these values, the time difference was $\Delta t = 1.83$s. This delay is within reach of some current detectors, like Fermi Gamma-ray space telescope, if we could identify low-energy and high-energy photon that left the source simultaneously.

2.2 Threshold anomaly

Modification to the modified dispersion relation also affects the propagation of particles through the vacuum. However, this medium is vacuum only in the first approximation since it's filled, among other things, with background photons.

In a classical scenario assuming the trivial dispersion relation, the collision of a high-energy photon (with energy E) with a low-energy background photon (with energy E_B), a reverse process to the electron-positron annihilation may occur as long as the energy of the high-energy photon satisfies

$$E > E_{th} = \frac{m_e^2}{E_b}. \tag{2.4}$$

This follows the conservation of four-momentum, and m_e is the mass of an electron. High-energy photons traversing distances on the order of megaparsecs or gigaparsecs interact with background or CMB photons (with $E_b = 10^{-3}$eV), resulting in attenuation. Yet, such high-energy photons have been detected from these distant sources, creating a paradox. One example of GRB reaching these energy scales is GRB 221009A, for which the distance was estimated to be 724Mpc with peak energies at least 18TeV.

2.2.1 Minimal mass of particle production

The interaction between two photons can create a particle with mass $m = \sqrt{EE_b/c^2}$. If m is smaller than the mass of any particle, interaction does not occur. Here, E_b is fixed, and it is the energy of the background photons. By increasing E, the mass of an electron is reached, and interaction is allowed to occur. Therefore, photons with sufficiently high energies disappear from the flux.

Considering the dispersion law (1.10), the finite value of E_F leads to a reduction in the obtainable mass. Consequently, even for very high energies E, the pair production process is suppressed, and the intergalactic space becomes effectively transparent.

The minimal mass of a particle produced by the high-energy photon with the momentum p as calculated in [5]

$$\begin{aligned} m &= \frac{1}{2c^2}\sqrt{E^2(p) - (pc)^2 + 2E_B(E(p) + pc)} \\ &= \frac{1}{2c^2}\sqrt{E_F^2\left(1 - \sqrt{1 - \frac{2pc}{E_F + 2pc}}\right)^2 - p^2c^2 + 2E_B\left(E_F\left(1 - \sqrt{1 - \frac{2pc}{E_F + 2pc}}\right) + pc\right)} \\ &\approx m_0\left(1 - \frac{3(pc)^2}{8E_F E_B}\right) + \cdots \end{aligned} \tag{2.5}$$

where $m_0 = \sqrt{pcE_B/c^2}$ is the unmodified threshold for the pair production. We now observe that the modified version reduces the obtained mass and suppresses the pair production. This result is sensitive to the chosen value of E_B.

Chapter 3

Gamma-ray data simulation

It is essential to create controlled and reproducible data sets to analyze the temporal behaviour of GRBs across different energy channels. Given the complex nature of real astronomical observations, we first simulate a set of synthetic GRB light curves based on physically motivated models.

The gamma ray burst simulation is governed by a set of parameters that define its spectrum and temporal characteristics. The parameters include spectral indices and specific energies to describe the band function 3.2 and time characteristics for the evolution of the GRB.

The simulation begins by constructing a temporal grid spanning an entire time range with evenly spaced time steps. The grid represents an observational window in which the GRB develops.

The GRB's behavior is then modeled using two concepts. The temporal evolution of GRB's intensity is characterized by a function that dictates its rise and decay. Prior to its peak, the intensity is defined by a simple power-law increase, and the post-peak intensity is modeled by a combination of power-law decay and exponential decay. The specific rates of rise, decay, and peak time are defined as the input parameters.

The spectral distribution of GRB emission is represented using the Band function, a widely used model for fitting GRBs. The function smoothly transitions between two power-law regimes at a defined peak energy. More about the Band function in section 3.2.

By combining the time-dependent light curve with the spectral model, the simulation calculates the expected photon flux at each moment in time across different energy bands. Each energy band is then integrated over the specified energy range. To recreate more realistic observational conditions, Poisson statistics are applied to generate photon counts at each point in time in each energy band. The final output is a set of simulated photon counts that encapsulates the expected trends and variability dictated by the initial model parameters.

Furthermore, for the purposes of this thesis, energy-dependent peak delay is added into the simulation. For each energy band, the peak time is determined linearly between a predefined minimum and maximum peak time based on the average energy of the bin.

3.1 Simulation method

The simulation is based on two core components

- **Spectral shape**: Modelled using band function, more described in 3.2, which describes the photon flux density set by a set of parameters
- **Temporal evolution**: Modelled using a parametric light curve function characterised by a rise phase controlled by the rise index and a decay phase, a power-law decay modulated by the exponential damping

The photon counts are then simulated across multiple predefined energy channels, each characterized by a lower and upper energy limit, and for each channel, an average energy value is determined the expected peak time of the flux.

The peak time t_{peak} for each energy is determined by linearly mapping the average energy to a temporal window defined by parameters t_{min} and t_{max} using equation

$$t_{\text{peak}} = t_{\text{peak,min}} + \frac{\langle E \rangle - E_{\text{min,tot}}}{E_{\text{max,tot}} - E_{\text{min,tot}}} \left(t_{\text{peak,max}} - t_{\text{peak,min}} \right). \tag{3.1}$$

This approach produces a systematic shift in the peak times, where higher-energy bands can exhibit different peak timings compared to lower-energy bands. This feature provides a controlled framework for testing analytical methods to detect and quantify peak time differences using current observational technologies.

The total flux over the energy range is computed using numerical integration. Photon counts for each energy band and each time step are then sampled from a Poisson distribution around the expected value given by the product of spectral flux, light curve, and a noise factor. The noise is modeled using Python's numpy library function *numpy.random.poisson* and then scaled down as needed for the analysis. The structure of the code is explained in the pseudocode below.

Algorithm 1 Simulation of GRB Light Curves

Load simulation parameters (spectral model, time bounds, energy bands, light curve shape)
Generate uniform time array t_i, $i = 1, \ldots, n$
for each energy band $[E_{\text{min}}, E_{\text{max}}]$ **do**
    Compute average energy $\bar{E}$
    Map $\bar{E}$ linearly to peak time t_{peak} within the allowed time window
for each time t_i **do**
    for each energy band **do**
        if $t_i < t_{\text{peak}}$ **then**
            Compute rising phase: $L(t_i) = (t_i / t_{\text{peak}})^r$
        else
            Compute decay phase: $L(t_i) = (t_{\text{peak}}/t_i)^d \times e^{-(t_i - t_{\text{peak}})/t_{\text{peak}}}$
        Calculate spectral flux $F(E)$ using the Band function
        Integrate $F(E)$ over $[E_{\text{min}}, E_{\text{max}}]$ to find expected photon counts
        Apply Poisson noise to simulate observed counts

3.2 Band Function

Gamma-ray bursts (GRBs) are the most luminous explosions in the universe, releasing energy in the form of gamma rays. A key aspect of analyzing GRBs is understanding their emission spectra, which is well described by the Band function introduced in [12]. The function is a smoothly broken power-law including a low energy component, a peak energy, and a high energy power law tail that best describes the spectral character of most GRBs. While the Band function is purely an empirical model, its physical origin has been subjected to an intense study in the past years. The function is still widely used to fit GRBs today.

Traditionally, the spectrum of GRBs has been connected to synchrotron radiation from relativistic electrons in the jet. The recent studies [14] suggest that shear particle acceleration in structured GRB jets plays a role in shaping the overall spectrum.

3.2.1 Mathematical formulation

The Band function describes the GRB photon spectrum $N(E)$ as a broken power law :

$$N(E) = \begin{cases} A\left(\frac{E}{100\,\text{keV}}\right)^{\alpha} e^{-E/E_0}, & E < (\alpha-\beta)E_0 \\ A\left(\frac{E}{100\,\text{keV}}\right)^{\beta} \left[\frac{(\alpha-\beta)E_0}{100\,\text{keV}}\right]^{\alpha-\beta} e^{(\beta-\alpha)}, & E \geq (\alpha-\beta)E_0, \end{cases} \tag{3.2}$$

where A is a normalization constant.

The low-energy index α describes how the GRB spectrum behaves at low photon energies. Energies below E_{peak}. Typical observed values are : $-1.5 \leq \alpha \leq -0.5$ [12] [13]. β, the high-energy spectral index, describes the steepness of the GRB spectrum at photon energies above E_{peak}. Typical values fall in the range: $-3.5 \leq \beta \leq -2.0$ [13]. The peak energy E_{peak} is the energy at which the νF_ν spectrum peaks. νF_ν is the spectral energy distribution representing the power per unit logarithmic frequency interval emitted by an astrophysical source, where ν is frequency and F_ν is the spectral flux density derived as $F_\nu = \frac{dF}{d\nu}$. The hardness of the spectrum is $E^2N(E)$ it is proportional to νF_ν and is related to the break energy E_0 by

$$E_{peak} = (2+\alpha)E_0. \tag{3.3}$$

E_{peak} represents the dominant energy scale of the GRB and is correlated with GRB luminosity and jet properties. Its values vary depending on the type of GRB, like long or short GRBs. Example of a spectrum of a GRB 1B91127 as fitted in [12] can be seen in figure 3.1.

3.2.2 Physical origin of the Band function

While the Band function is a great empirical fit, its physical origin is still debated. In standard models, the GRB is linked to synchrotron radiation from electrons accelerated in internal shocks within the relativistic jet. In contrast, [14] proposes a structured jet model in which the GRB consists of a Jet Core and a Mixed Jet-Cocoon. In picture 3.2 we can see the GRB jet core structure and cocoon structure.

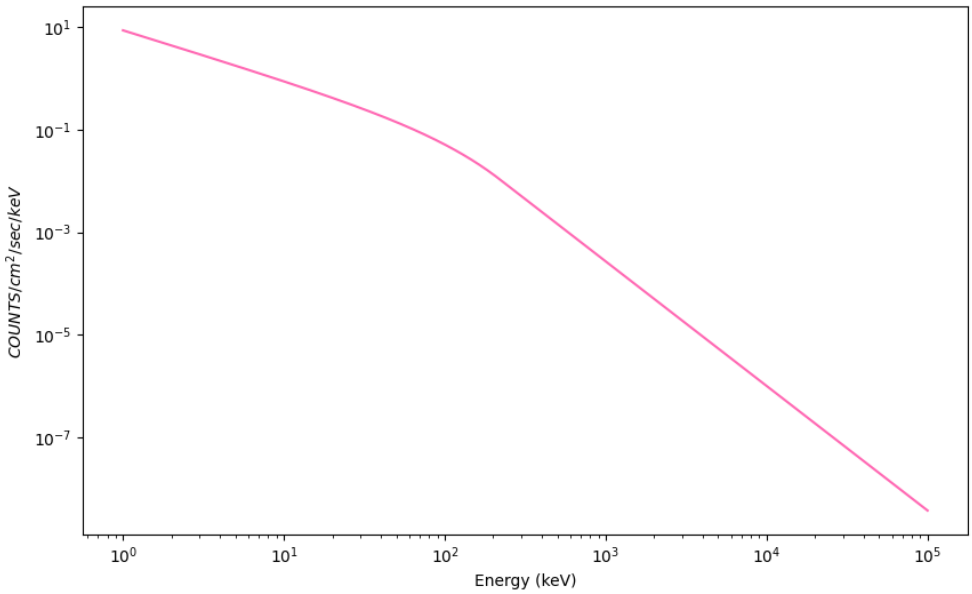

Figure 3.1: Spectrum of GRB 1B91127 fitted by [12] with $\alpha = -0.968$, $\beta = -2.427$, and break energy $E_0 = 149.5$

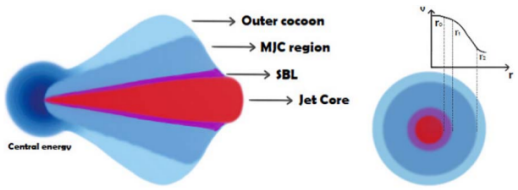

Figure 3.2: The schematic diagram of the jet-cocoon structure. [14]

Jet Core

This is a narrow, highly collimated outflow with ultrarelativistic speed. In the core, internal shocks occur as shells of material with slightly different speeds collide. These shocks are sites for efficient particle acceleration via first-order Fermi acceleration. This leads to a population of electrons with a broken power-law energy distribution. The intense magnetic fields in the core (typically $B_{jet} \sim 10^6 G$)[14] enable these electrons to produce synchrotron radiation that dominates the keV-MeV portion of the spectrum.

Mixed Jet-Cocoon

A transitional zone between the jet core and the surrounding cocoon. It's characterized by a radially decreasing velocity profile. This velocity shear provides a mechanism for shear acceleration. Electrons injected into the MJC region gain energy as they repeatedly cross layers with different velocities, leading to an electron energy distribution distinct from that produced by shocks. The MJC region emits both via synchotron radiation and through the synchotron self-Compton process, where photons are upscattered by the same population of electrons into higher energies.

The combined emission from the jet core and the MJC region results in the overall spectral energy distribution that is well described by the band function. The smooth break in the spectrum and the presence of the additional components (such as X-ray excess) are a natural consequence of the interplay between shock and shear acceleration. [14] applies this model to explain the prompt gamma-ray spectra of bright GRBs 090926A, 131108A, and 160509A, whose spectra distinctly show two components or a Band cut function shape.

Chapter 4

Delay detection

In the previous chapter, we detailed the simulation of GRB data incorporating an energy-dependent dispersion. Here, we develop and compare two methods for detecting the introduced delay. The first method is the traditional cross-correlation, which, while widely used, suffers from limited sensitivity when the delay is smaller than the temporal bin width used to collect the data. To overcome this limitation, we introduce a new method, here referred to as error-correlation, this method predicts the counts in higher energy channels and compares them to the actual channel counts. We aim to reveal the subtle correlation structure introduced by the dispersion.

In this chapter, we outline the data analysis techniques: we explain the conventional cross-correlation approach and introduce the error-correlation method, which systematically scans for time shifts by analyzing the correlation between residuals in consecutive time bins. Finally, we present results from both methods, discuss their relative performance, and consider the challenges of detecting such small delays.

4.1 Cross-correlation

Cross-correlation is a fundamental method in signal processing, statistics, and time series analysis. It is a measure of similarity of two series as a function of displacement of one relative to the other and is essential for detecting time shifts, periodicities, or the degree of similarity between two signals.

4.1.1 Definition

For two discrete signals $x[t]$ and $y[t]$ the cross-correlation function $r_{xy}[k]$ is defined as

$$r_{xy}[k] = f(x \star y)[n] = \sum_{t=-\infty}^{\infty} x[n]y[n+k], \tag{4.1}$$

the parameter k is the lag or time shift between the two signals. A value of $k = 0$ corresponds to no shift, while positive or negative values correspond to shifting one signal relative to another. Similarly, for continuous signals it is defined as

$$r_{xy}(k) = f(x \star y)(k) = \int_{-\infty}^{\infty} x(t)y(t+k)dt. \tag{4.2}$$

In many applications, it is useful to normalize the cross-correlation to obtain a value between −1 and 1. This normalization is analogous to the Pearson correlation coefficient for two signals. A common normalization is

$$\rho_{xy}[k] = \frac{r_{xy}}{\sqrt{r_{xx}[0] r_{yy}[0]}}, \tag{4.3}$$

where $r_{xx}[0]$ and $r_{yy}[0]$ are the auto-correlations at zero lag, which represent the variance of the signal. The logic of my cross-correlation calculation code is shown in the pseudocode below.

Algorithm 2 Cross-Correlation Analysis Method

1: **for** each pair of energy bands (C_i, C_j) **do**
2: Compute discrete cross-correlation $(C_i * C_j)(\tau)$
3: Identify lag $\tau_{\max}$ where cross-correlation is maximum
4: Retrive time lags relative to the lowest energy band
5: Perform linear regression to model:
measured lag τ_j as a linear function of energy E_j
6: Fit model: $\tau_j = a \times E_j + b$
7: Calculate residuals: $\Delta\tau_j = \tau_j - (aE_j + b)$

4.2 Error-correlation

According to certain quantum gravity theories, high-energy photons could travel at slightly different speeds compared to their lower-energy counterparts, resulting in subtle time delays in their arrival times.

In this chapter, we present a method for detecting such time delays using an error correlation analysis approach. Unlike traditional cross-correlation techniques that may be limited by the temporal resolution of the data, our method leverages the prediction error between a low-energy reference channel and higher-energy channels. By analyzing the normalized correlations of these errors at different time lags, we aim to reveal systematic shifts that could indicate the presence of vacuum dispersion.

4.2.1 Theory

Observations of GRBs are typically recorded as photon counts in discrete time intervals (time bins). Each bin represents an integrated photon count over a short period. In addition, photon counts are measured across multiple energy channels that cover different energy ranges. In our analysis, we assume that the lowest energy channel is least affected by the vacuum dispersion and, therefore, can serve as a reference channel.

In GRB observations, the data are collected in discrete time bins T_{bin}. Under the null hypothesis, these channels are time-aligned. But can differ in total amplitude or noise amplitude. However, if a delay Δt exists and $\Delta t < T_{bin}$ a small fraction of photons $\delta = \Delta t / T_{bin}$ ends up in the next bin. The number of these photons can be very small, even $\delta = \Delta t \cdot N_{bin} < 1$.

First, we predict the counts in the higher energy channel. Assuming that the channels differ only in the scaling factor, the predicted counts for channel two in time t are given by 4.4.

$$N_2^P(t) = N_1(t) \cdot \frac{\langle N_2 \rangle}{\langle N_1 \rangle}, \tag{4.4}$$

where the $N_1(t)$ is the photon count in the reference channel at time t and $\langle N_1 \rangle$, $\langle N_2 \rangle$ are the mean counts over all bins in channel 1 and channel 2, respectively. The scaling factor takes care of the different amplitudes.

Now, we can take the prediction of N_2^P and the real value of N_2 as two random and independent data points and check how wrong our estimate was by computing

$$\varepsilon(t) = N_2^P(t) - N_2(t).$$

In the absence of any time delay, the residuals $\varepsilon(t)$ are expected to be random and uncorrelated from bin to bin.

When a small delay is present, a fraction of photons, approximately $\delta \cdot N_{bin}$, does not fall into the expected bin but is recorded in the subsequent bin. This causes the residual in one bin to decrease (if photons are lost) and the residual in the following bin to increase (if photons are gained). This method quantifies this effect by calculating the correlation between residuals in selected bins

$$C = \langle \varepsilon(t) \cdot \varepsilon(t+\tau) \rangle \tag{4.5}$$

Under zero delay, this correlation is expected to be near zero (or at a baseline level determined by noise). However, if a delay is present, the asymmetry in the residuals between successive bins will lead to a significant deviation of $C(t)$ from zero. How the error-correlation is calculated in my code is shown in the pseudocode below.

Algorithm 3 Error Correlation Analysis Method

1: Select the lowest energy band as the reference channel C_{ref}
2: **for** each higher energy channel C_j **do**
3: Estimate predicted counts as:
$$C_j^{\text{predicted}}(t) = C_{\text{ref}}(t) \times \frac{\text{mean}(C_j)}{\text{mean}(C_{\text{ref}})}$$
4: Calculate prediction error:
$$\varepsilon_j(t) = C_j^{\text{predicted}}(t) - C_j(t)$$
5: **for** each lag τ **do**
6: Compute lagged normalized error correlation:
$$r_j(\tau) = \frac{\frac{1}{n-\tau}\sum_{t=0}^{n-\tau-1}[\varepsilon_j(t)\varepsilon_j(t+\tau)]}{\frac{1}{n}\sum_{t=0}^{n-1}[\varepsilon_j(t)^2]}$$
7: Collect $r_j(\tau)$ for all channels and all lags

Chapter 5

Interpretation of results

5.1 Simulated Data

The primary objective of this chapter is to present the simulated datasets used to evaluate the performance of two delay detection methods: cross-correlation and residual error correlation. Since real gamma-ray burst (GRB) data are often affected by limited resolution, observational noise, or incomplete energy coverage, a controlled simulation framework is essential. It allows us to systematically test under which conditions a time delay between energy channels can be detected, and where the methods fail.

Each dataset represents a synthetic GRB event generated using a Band function spectrum, combined with a time-dependent intensity profile and a tunable, energy-dependent peak time delay. Across multiple simulation runs, three key variables were systematically varied:

- **Temporal resolution** — to simulate different observational instruments,
- **Noise level** — to assess robustness to statistical fluctuations,
- **Injected delay magnitude** — to evaluate detection thresholds for both methods.

Band Function Parameters

The spectral shape of the GRB was modeled using the Band function with fixed parameters across each dataset. These parameters were based on real spectral fits from some of the most energetic GRBs observed. Multiple light curves were generated for each configuration by varying the temporal resolution. Within each such subset, the injected peak delay between energy channels was gradually reduced to test the sensitivity limits of the detection algorithms. Lastly, everything was also generated with scaled-down and without noise levels to further test the limits of the methods

Each combination of parameters was run independently to evaluate both detection methods in a variety of scenarios, from ideal noiseless data to low-resolution, high-noise data mimicking weak GRBs. In the figure below 5.1 are simulated light curves with Band parameters of GRB 221009A [11].

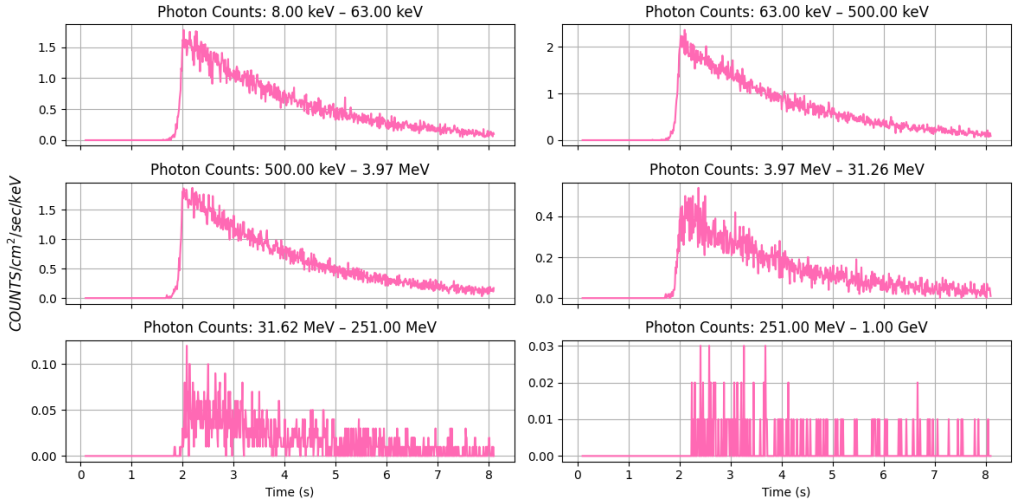

Figure 5.1: Simulated GRB light curves with band parameters of GRB 221009A with photon noise scaled to 5%.

5.2 Poisson (Photon) Noise

Photon noise arises from the discrete, independent arrival of photons [20]. If the expected number of photons in a time bin is μ, the probability of measuring exactly N photons is

$$P(N;\mu) = \frac{\mu^N e^{-\mu}}{N!}, \tag{5.1}$$

with

$$\mathbb{E}[N] = \mu, \qquad \mathrm{Var}[N] = \mu, \tag{5.2}$$

so that the signal-to-noise ratio scales as

$$\mathrm{SNR} = \frac{\mu}{\sqrt{\mu}} = \sqrt{\mu}. \tag{5.3}$$

Thus, although absolute fluctuations grow with the signal, the relative noise decreases as photon counts increase, setting a fundamental, signal-dependent floor on measurement accuracy.

In the simulation, we take the model's ideal counts per bin, multiply them by a single `noise_factor` to form the Poisson rate parameters, draw independent Poisson samples, and then divide by `noise_factor` to restore the original scale. By increasing `noise_factor`, the relative noise decreases; by decreasing it, the noise increases. This is how we can control SNR in the code.

5.3 Cross-correlation method results

The first method tested for detecting energy-dependent time delays in the simulated GRB data was cross-correlation. This classical signal processing technique is widely used to estimate time shifts between two signals. It is particularly suitable for cases where the signals share a similar shape but may be offset in time.

Methods

For each simulated GRB dataset, the cross-correlation function was computed between the photon count time series of the high-energy and low-energy channels. The aim was to determine the lag that maximizes the similarity between the two signals. This was done using the normalized cross-correlation, which measures the similarity while accounting for variations in amplitude and scale.

The maximum of the cross-correlation function gives the estimated lag between channels, expressed in units of time bins. A peak at lag = 0 indicates that the signals are synchronized, while a peak at lag = 1 or more indicates that one channel leads or lags the other by a full time bin.

This procedure was applied to each simulation run across different noise levels, temporal resolutions, and injected delay values. Special attention was given to comparing the lowest and highest energy channels, where the artificial delay introduced in the simulation was the most pronounced.

The results show that the cross-correlation method performs well when the introduced delay is equal to or greater than the size of a time bin. In these cases, the method consistently identifies the correct lag between energy channels. When the delay is smaller than one bin, the method occasionally detects a shift, but the estimated delay is often inaccurate due to its limited resolution. As the delay decreases further, the method typically fails to register any shift at all and incorrectly indicates that the signals are synchronized. This confirms that cross-correlation is fundamentally limited to detecting delays no smaller than one time bin.

Figures 5.2 and 5.5 compare the injected time delays with those recovered by the cross-correlation method on the same light-curve data, first with Poisson noise at the 1% level and then at 50%. As these plots show, when the noise level is high, even cross-correlation cannot reliably recover the true delay.

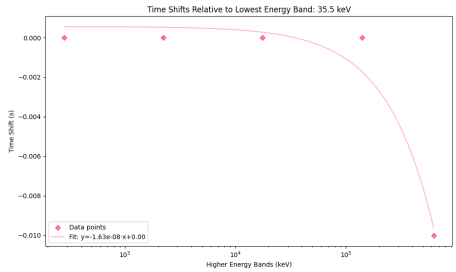

(a)

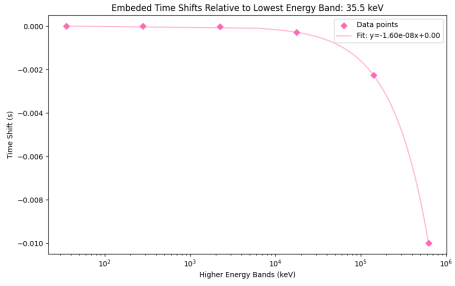

(b)

Figure 5.2: (a) Delay detected by cross-correlation relative to the lowest energy channel. (b) Delay input to the simulated data was tested on an 8-second GRB with a temporal resolution of 0.01 seconds. With Poisson noise scaled down to 1% its original value.

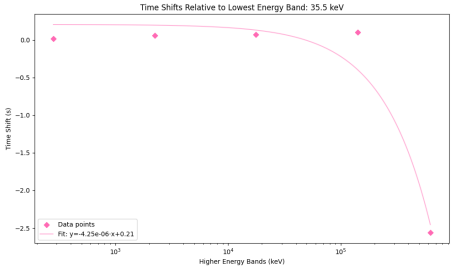

(a)

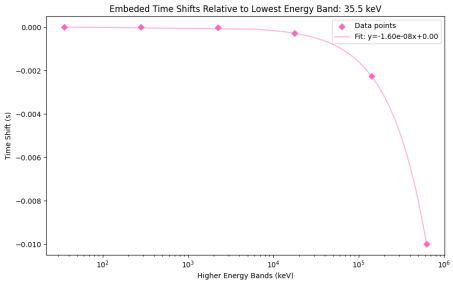

(b)

Figure 5.3: (a) Delay detected by cross-correlation relative to the lowest energy channel. (b) Delay input to the simulated data tested on an 8-second GRB with a temporal resolution of 0.01 seconds and Poisson noise scaled down to 50%.

5.4 Error-correlation method results

While the error correlation method shows theoretical potential for detecting small energy-dependent time delays between energy channels, it currently does not provide a reliable or accurate estimate of the delay in time units, especially when observational noise is present.

The method is based on computing prediction errors between a reference energy channel and others, and then evaluating the correlation of those residuals at different time lags. In the ideal case, with no noise and well-defined delay, a clear pattern of correlation emerges, typically peaking at the lag corresponding to the approximate time offset. This has been observed in noiseless simulations with injected sub-bin delays, where the correlation function shows a distinguishable structure not captured by the classical cross-correlation method.

However, in more realistic scenarios involving statistical fluctuations or background noise, this structure quickly disappears. Even moderate levels of Poisson noise significantly reduce the correlation signal, making it difficult to distinguish true temporal shifts from random variations in photon counts. As a result, the method fails to provide consistent or trustworthy estimates of the delay under noisy conditions, which are typical in gamma-ray burst (GRB) observations.

In Figure 5.4, I present four detections from error-correlation, all tested on data with the same Band function parameters but different delays and noise levels. When some delay is detected, the correlation seems to be going up, indicating a steady error at t and $t + \tau$. However, when presented with higher levels of noise, the method fails before the cross-correlation. The length of the burst was 8s, the temporal resolution was 0.01 seconds, and the delay for tests in figure 5.4 was set to 0.04 seconds, so the method had a problem detecting the delay even when the delay was larger than the size of the time bin.

Although the method shows great sensitivity when no noise is added to the simulation. Comparison of error-correlation on the same data set, one with delay present and the other when not, is shown in figure 5.5.

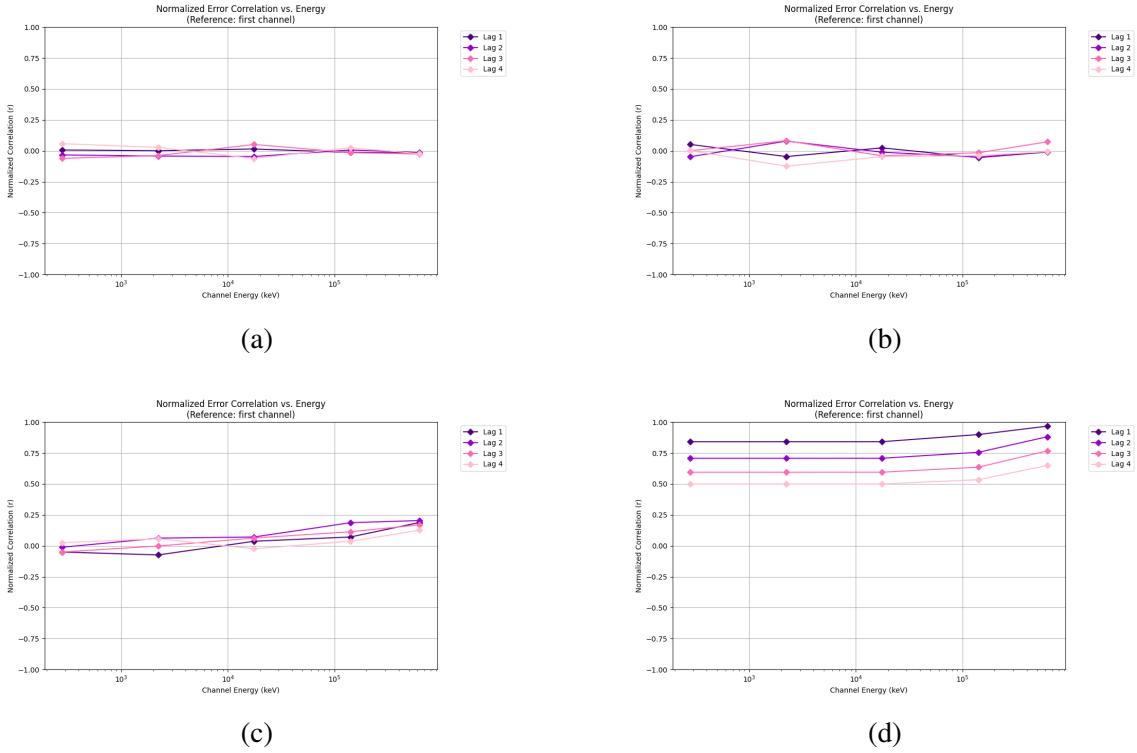

Figure 5.4: Error-correlation method for detecting delay tested on simulated GRB light curve with length of 8 seconds, temporal resolution 0.01 seconds and embedded delay 0.04 seconds through the energy channels with the Poisson noise scaled down to for (a) 50%, (b) 10%, (c) 1% and (d) without noise

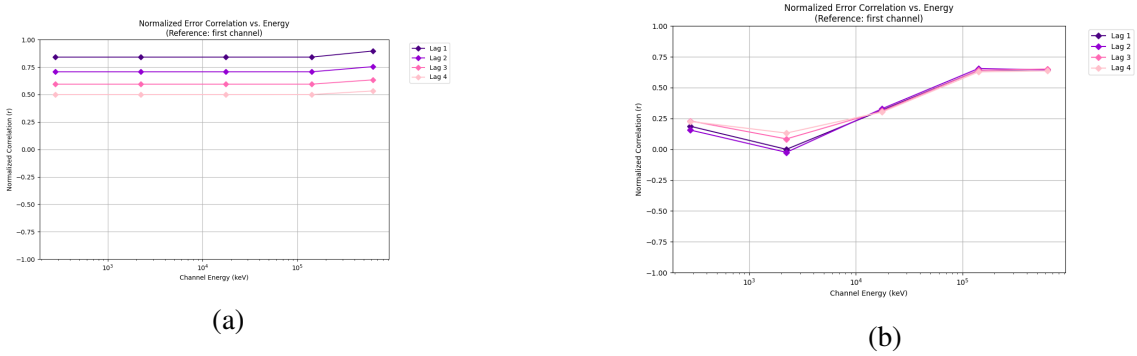

Figure 5.5: Error-correlation method for detecting delay tested on simulated GRB light curve with length of 8 seconds, temporal resolution 0.01 seconds, and embedded delay just 0.003 seconds in (a) and 0 in (b)

5.5 Comparison

Based on the tests, with the noise present, the cross-correlation seems to be performing better; however, when the noise becomes too big, even the cross-correlation can't retrieve the delay. In this section, I provide some comparisons of how both of these methods

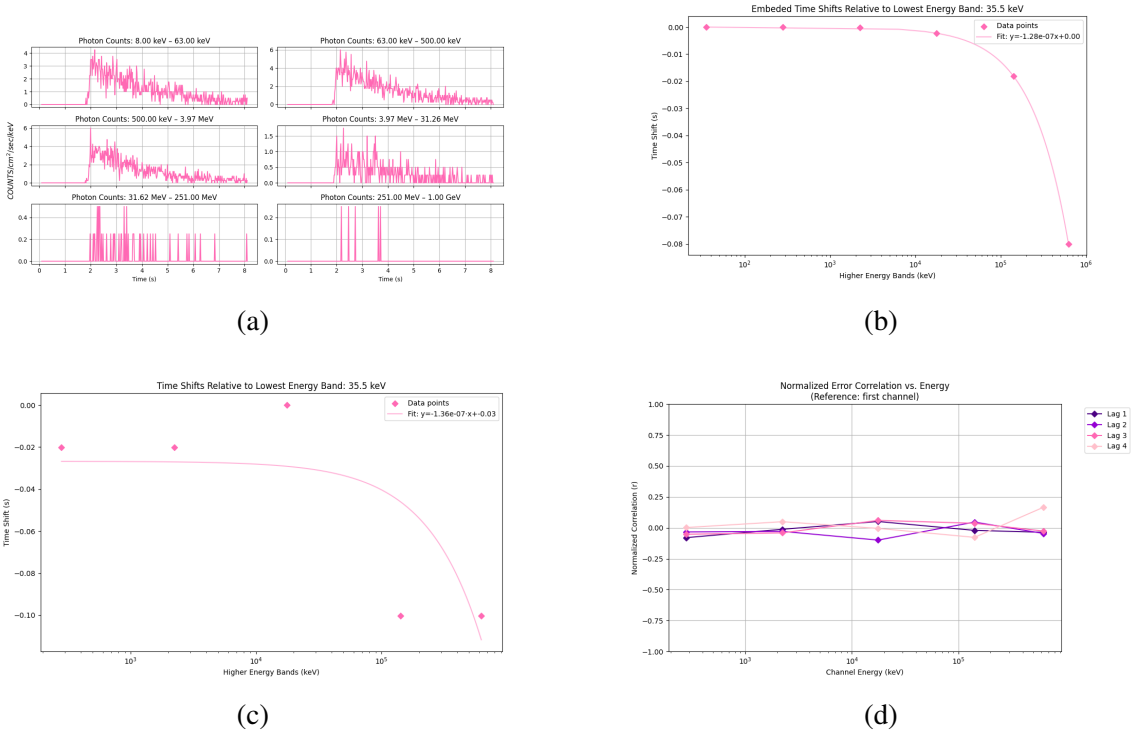

Figure 5.6: (a) Simulated GRB lightcurve data with Poisson noise scaled down to 50% and time bin width 0.02 seconds, (b) the input delay, (c) cross-correlation results, (d) error-correlation results.

performed in various conditions.

In figure 5.6 as we can see the noise was relatively low in high energy channels as the time-bin size was big and enough photons could be detected, but as the counts in high energy channels become lower, the noise dominates the simulation and both methods fail to detect the delay. We can see a similar result in figure 5.8 where the noise was scaled down even lower, but since the size of the time-bin was much smaller, the counts were low and noise again dominated in the higher energy channels.

In figure 5.7, the noise was set low, and by error-correlation, we can see a slight peak in the first lag, indicating a sub-bin size delay. These data are, however, very clean and unrealistic from a real observation.

5.6 Future of phenomenological quantum gravity

Over the past two decades, theoretical proposals in quantum gravity phenomenology have matured into observational considerations. The foundational ideas proposed in the late 90s in [15] have since inspired a wave of experimental efforts to detect these effects using data from GRBs or other high-energy sources.

With the continued evolution of instrumentation and satellite technology, the future of phenomenological quantum gravity rests on the development and deployment of highly specialised observatories. The next-generation missions must combine wide energy coverage,

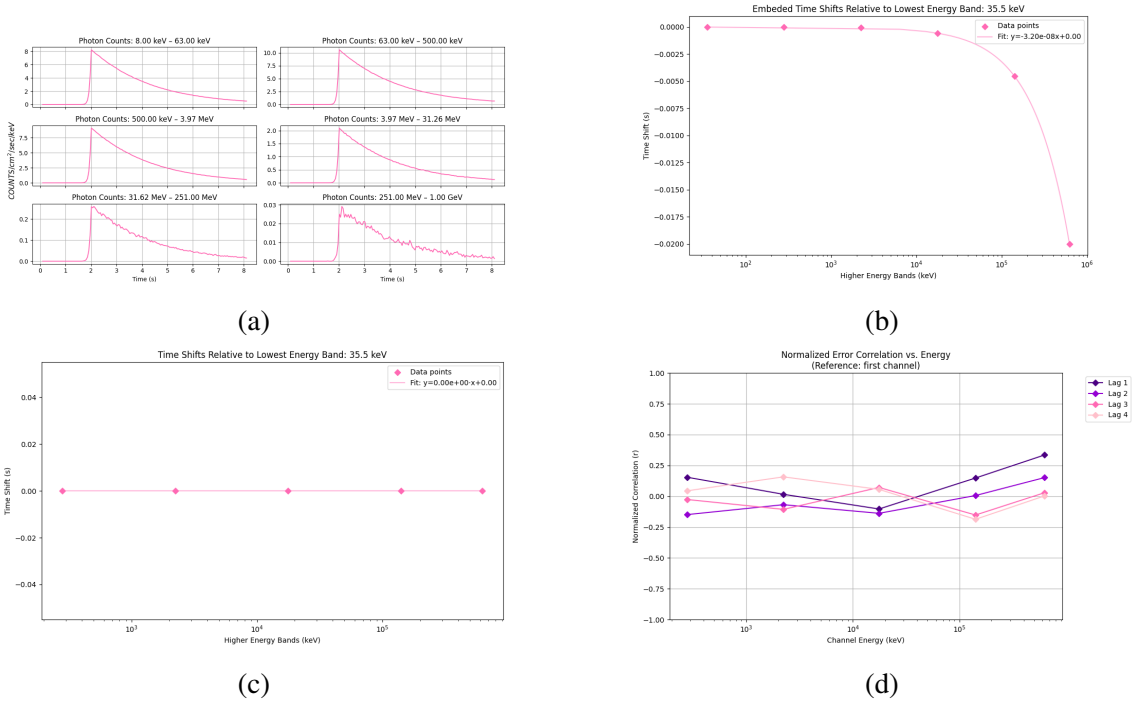

Figure 5.7: (a) Simulated GRB lightcurve data with Poisson noise scaled down to 1% and time bin width 0.05 seconds, (b) the input delay, (c) cross-correlation results, (d) error-correlation results.

high temporal resolution, and cosmological distance reach.

Space-based and ground-based telescopes are being explicitly designed to address the core questions of phenomenological quantum gravity. The Fermi Gamma-ray space telescope, operational since 2008, has already provided some constraints on the observation of Lorentz invariation variation through its observations of short GRBs, most notably GRB 090510. The lack of detectable delay between photons of different energies placed lower bounds on the quantum gravity energy scale exceeding 10^{19}GeV [16]. The next frontier, however, lies in the mission optimised for detecting tiny dispersion effects.

5.6.1 Grail Quest

Grail Quest is a flagship-scale mission to investigate quantum gravity via high-energy transients. According to [17], the mission was submitted for consideration within ESA's Voyage 2050 program. As of 2025, the mission is still not formally approved or funded; however, it continues to represent one of the most ambitious experimental frameworks for probing quantum gravity phenomenology using gamma ray bursts.

At its core, Grail Quest proposes to deploy a constellation of hundreds to thousands of 3U-6U nanosatellites, each located at low Earth orbit. As proposed in [17] every satellite would be equipped with :

- an array of GAGG (Gadolinium-Aluminium-Gallium Garnet) crystal scintillators for detecting gamma-rays in the 20 keV to several MeV range,

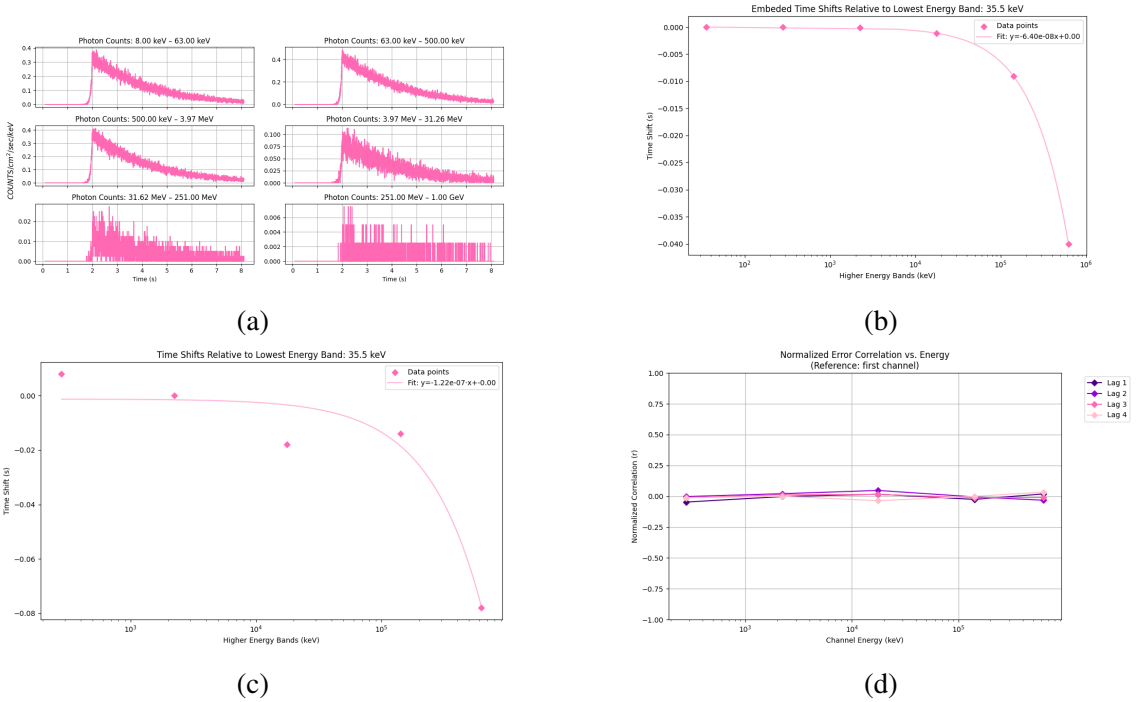

Figure 5.8: (a) Simulated GRB lightcurve data with Poisson noise scaled down to 5% and time bin width 0.002 seconds, (b) the input delay, (c) cross-correlation results, (d) error-correlation results.

- Silicon Drift Detectors (SDDs) surrounding the scintillators for additional sensitivity in the soft X-ray range,
- tungsten shielding on the detector housing to suppress background noise from cosmic X-rays and particle interactions,
- an ultra-precise onboard timing system, capable of resolving photon arrival times down to 10–100 nanoseconds.

These detectors would operate independently but coordinate via GPS and inter-satellite coordination links, allowing for temporal triangulation of high-energy photon arrivals across the constellation. This architecture transforms the fleet of satellites into a single synthetic instrument with a collective effective area and field of view far superior to any single satellite observatory.

5.6.2 Mission HERMES

The HERMES (High Energy Rapid Modular Ensemble of Satellites) missions represents one of the most innovative experimental platforms in modern high-energy astrophysics [18]. Conceived as a pathfinder for larger constellation-based missions, HERMES is a distributed network of nanosatellites designed to detect and localise GRBs and other high-energy transients using high-precision timing techniques. Notably, HERMES is the first

mission designed to use temporal triangulation to reconstruct the position of astrophysical events with high angular precision, without relying on onboard imaging.

The HERMES comprises a fleet of 3U CubeSats $30 \times 10 \times 10$ centimeters, deployed in low Earth orbit. The advantage of this architecture lies in its modularity. A failure of one satellite does not compromise the mission's capabilities, as the remaining units continue to operate independently. Each satellite will be equipped with:

- A GAGG (Gadolinium-Aluminium-Gallium Garnet) scintillator array for gamma-ray detection in the 20 keV to 0.5 MeV range,
- An array of Silicon Drift Detectors (SDDs) integrated within the scintillator blocks to detect soft X-rays between 2 keV and 20 keV,
- Tungsten shielding around the sides and bottom of the detectors to minimise background noise from the cosmic X-ray background,
- A high-precision GPS-synchronised clock providing timing accuracy at 100 microseconds, crucial for both source localisation and time-of-flight measurements.

HERMES has been conceived with three primary scientific goals in mind. To detect and localise high-energy transients with an accuracy of several arcminutes. To investigate GRB emission mechanisms by capturing the prompt emission phase with high timing precision, HERMES can help to resolve the substructure of GRB light curves. And most importantly for us and the most ambitious goal is the search for quantum gravity effects, particularly through in vacuo dispersion.

The HERMES Pathfinder launched as part of the SpIRIT mission in 2023 and has already demonstrated in-orbit functionality [19]. The successful operation of these units validates the feasibility of the full HERMES constellation.

Conclusions

In this thesis, we presented a comprehensive, step-by-step simulation and analysis pipeline to assess the detectability of tiny, energy-dependent arrival-time shifts in gamma-ray burst light curves. We began by describing our framework for generating synthetic bursts in multiple energy channels, imposing controlled, linear delays proportional to photon energy, and then applying Poisson noise to simulate realistic photon statistics. We systematically varied three key observational parameters: noise levels, time-shift between energy channels, and temporal resolution to produce a suite of datasets spanning injected delays from several time bins down to sub-bin scales.

We then applied and compared two delay-detection algorithms. The classical cross-correlation method reliably recovers whole-bin delays when photon counts are high but fails to resolve sub-bin shifts or in lower-count regimes.The cross-correlation required the noise to be scaled down to at least 10% of its original value to be able to reliably detect delay.

The novel error-correlation technique, by predicting high-energy counts from the low-energy channel, computing residuals, and examining their lagged autocorrelation, achieves sub-bin sensitivity when the noise is scaled down to 1% or lower, otherwise shows lower sensitivity than cross-correlation. In its present form, the method serves more as a qualitative indicator than a quantitative tool. It can suggest the presence of a small delay in idealized, clean data, and under such conditions, it shows greater sensitivity than cross-correlation. But it cannot currently extract the actual delay value, especially not in seconds or with sub-bin precision, and it fails in the presence of even moderate noise. In summary, while the error correlation method represents a conceptually interesting approach, its current implementation is limited to noise-free simulations and offers no practical advantage over existing methods when applied to real or noisy data.

By mapping each method's detection threshold across our parameter grid, we quantified the trade-offs inherent in observational design. Finer time bins improve sub-bin recovery yet raise statistical noise. A wider energy range could help with the delay detection as it would increase the predicted delay between low- and high-energy channels. These results translate into quantitative guidelines and show that current instruments with millisecond timing and moderate effective area could probe delays only in bright, low-noise, spectrally broad bursts.

We recognize several limitations that future studies should address: our use of simple, single-pulse light curves and linear delay models omits complex spectral evolution and multi-pulse structure, and our noise modeling neglects instrumental noise. Follow-on work should incorporate realistic instrument noise and apply this validated framework to archival GRB datasets to derive empirical constraints on energy-dependent photon dispersion.

Overall, this thesis establishes a transparent, reproducible blueprint for simulating GRB observations, benchmarking delay-detection methods, and defining the observational regimes required to test phenomenological models of quantum gravity-induced dispersion.

Bibliography

[1] Claus Kiefer. (2023). *A Review on Quantum Gravity*. arXiv:2302.13047 [gr-qc]. Retrieved from https://arxiv.org/pdf/2302.13047

[2] Planck Collaboration, Aghanim, N., Akrami, Y., Ashdown, M., Aumont, J., Baccigalupi, C., et al. (2018). Planck 2018 results. VI. Cosmological parameters. *Astronomy & Astrophysics*, **641**, A6. https://doi.org/10.1051/0004-6361/201833910

[3] Becker, K., Becker, M., & Schwarz, J. H. (2006). *String Theory and M-Theory: A Modern Introduction*. Cambridge University Press.

[4] Sotiriou, T. P. (2013). Gravity and scalar fields. *Living Reviews in Relativity*, **16**, 2. https://doi.org/10.12942/lrr-2013-2

[5] Kovačik, S., Důríšková, M., & Rusnák, P. (2024). Phenomenology of the dispersion law in a three-dimensional quantum space. *International Journal of Modern Physics A*, **2024**.

[6] Kovačik, S., & Prešnajder, P. (2018). The velocity operator in quantum mechanics in noncommutative space. arXiv:1309.4592 [math-ph]. https://arxiv.org/abs/1309.4592

[7] Addazi, A., Alvarez-Muñiz, J., Alves Batista, R., Amelino-Camelia, G., Antonelli, V., Arzano, M., et al. (2022). Quantum gravity phenomenology at the dawn of the multi-messenger era — A review. *arXiv preprint* arXiv:2111.05659. https://arxiv.org/abs/2111.05659

[8] Li, H., & Ma, B.-Q. (2023). Searching Lorentz invariance violation from cosmic photon attenuation. *The European Physical Journal C*, **83**, 192. https://doi.org/10.1140/epjc/s10052-023-11334-z

[9] Amelino-Camelia, G. (2002). Quantum gravity phenomenology: Status and prospects. *arXiv preprint* hep-th/0204051. https://arxiv.org/abs/gr-qc/0204051

[10] Amelino-Camelia, G. (2013). Quantum-spacetime phenomenology. *Living Reviews in Relativity*, **16**, 5. https://doi.org/10.12942/lrr-2013-5

[11] Burns, E., Svinkin, D., Fenimore, E., Kann, D. A., Agüi Fernández, J. F., Frederiks, D. D., et al. (2023). GRB 221009A: The BOAT. *The Astrophysical Journal Letters*, **946**(1), L31. https://doi.org/10.3847/2041-8213/acc39c

[12] Band, D., Matteson, J., Ford, L., Schaefer, B., Palmer, D., Teegarden, B., et al. (1993). BATSE observations of gamma-ray burst spectra. I. Spectral diversity. *The Astrophysical Journal*, **413**, 281–292. https://doi.org/10.1086/172995

[13] Guiriec, S., Kouveliotou, C., Daigne, F., Zhang, B., Hascoët, R., Nemmen, R., & Thompson, D. (2015). Toward a better understanding of the GRB phenomenon: A new model for GRB prompt emission. *The Astrophysical Journal*, **807**(2), 148. https://doi.org/10.1088/0004-637X/807/2/148

[14] Wang, Z.-Q., Huang, X.-L., & Liang, E.-W. (2024). Shear particle acceleration in structured gamma-ray burst jets. I. Physical origin of the Band function and application to GRBs 090926A, 131108A, and 160509A. *The Astrophysical Journal*, **977**, 182. https://doi.org/10.3847/1538-4357/ad93cb

[15] Amelino-Camelia, G., Ellis, J., Mavromatos, N. E., Nanopoulos, D. V., & Sarkar, S. (1998). Tests of quantum gravity from observations of gamma-ray bursts. *Nature*, **393**(6687), 763–765. https://doi.org/10.1038/31647

[16] Ackermann, M., Asano, K., Atwood, W. B., et al. (2009). A limit on the variation of the speed of light arising from quantum gravity effects. *Nature*, **462**, 331–334. https://doi.org/10.1038/nature08574

[17] Burderi, L., Di Salvo, T., Riggio, A., Sanna, A., & Iaria, R. (2021). GrailQuest: Hunting for atoms of space and time hidden in the wrinkle of space–time. *Experimental Astronomy*, **51**, 183–205. https://doi.org/10.1007/s10686-021-09745-5

[18] Fuschino, F., Fiore, F., Malaguti, G., et al. (2022). The HERMES pathfinder mission for time-domain astrophysics. *Galaxies*, **10**(1), 4. https://doi.org/10.3390/galaxies10010004

[19] Trenti, M., del Castillo, M. O., Mearns, R., et al. (2024). SpIRIT mission: In-orbit results and technology demonstrations. *arXiv preprint*, arXiv:2407.14034. https://arxiv.org/pdf/2407.14034

[20] Hasinoff, S. W. (2014). Photon, Poisson noise. In K. Ikeuchi (Ed.), *Computer Vision*. Springer, Boston, MA. https://doi.org/10.1007/978-0-387-31439-6$_4$82

For the codes and all generated data, and graphs, scan/click the QR code